On the Origin of Electrochemical Oscillations at Silicon Electrodes

Conclusions

We investigated the thermocharge and discharge characteristics and the cycling performance of a thermochargeable galvanic cell with carbon fiber main electrodes, a $[Fe(CN)_6]^{4-/3-}$ redox couple, a cation exchange membrane, and an extra pair of carbon fiber electrodes. The following results were obtained.

1. The Seebeck coefficient dE/dT of the experimental cells changed depending on the distance between the main electrodes. The absolute value $|dE/dT|$ of cell B (1.9 cm between the main electrodes) was about twice that for cell A (1.1 cm between the main electrodes) when the temperature difference (δT) between the holders for the main electrodes was more than 60°C.

2. The ratio of discharge capacity at 0.5 mA/cm^2 to thermocharge capacity at 0.1 mA/cm^2 was more than 90% when there was a temperature difference between the main electrode holders. The cell showed good thermal energy storage. And even when discharging after δT fading, the ratio stayed above 80% at $\delta T > 35$°C during thermocharging. However, the ratio in the latter case depended on δT. This may be because of a large temperature difference between the extra electrodes. On the other hand, thermocharge capacity strongly depended on the thermal condition. The thermocharge capacity during δT fading was at most 21% of that at constant δT. The cell is not expected to be thermocharged sufficiently when no thermal energy is supplied.

3. The cell showed good thermocharge and discharge cycleability. Thermocharge and discharge capacities were mostly maintained at constant values for over 40 cycles, although electrolyte leakage occasionally terminated the cycling.

4. The cell can be discharged from the extra electrodes at constant voltages while simultaneously thermocharging at the same current from the main electrodes. The cell was simultaneously thermocharged and discharged at 0.5 mA/cm^2 and constant voltages of the main and extra electrodes for over 1000 hours.

5. As a thermoenergy conversion system, our cell showed nearly the same thermal efficiency and power density as the conventional thermocell.

Manuscript submitted Sept. 5, 1995; revised manuscript received Dec. 5, 1995.

NTT assisted in meeting the publication costs of this article.

REFERENCES

1. W. Vielstich, *Fuel Cells*, pp. 345-361, Wiley-Interscience, New York (1960).
2. A. D. Payton, B. H. Boyd, C. M. Houck, E. H. Temple, and A. H. Zimmerman, *This Journal*, **120**, 373 (1973).
3. D. D. Macdonald, A. C. Scott, and P. Wentreck, *ibid.*, **126**, 1618 (1979).
4. A. D. Payton, E. J. Amis, S. Showell, R. W. Smith, and B. D. Koplitz, *ibid.*, **127**, 2157 (1980).
5. H. L. Chum, R. F. Fahlsing, and T. S. Jayadev, in *Proceedings of Interscience Energy Conversion Engineering Conference*, **15**, 1603 (1980).
6. B. Burrows, *ibid.*, **10**, 821 (1975).
7. B. Burrows, *This Journal*, **123**, 154 (1976).
8. T. I. Quickenden and C. F. Vernon, *Solar Energy*, **36**, 63 (1986).
9. T. Ikeshoji, *Bull. Chem. Soc. Jpn.*, **60**, 1505 (1987).
10. T. Ikeshoji and F. N. Nahui, *J. Electroanal. Chem.*, **296**, 19 (1990).
11. A. V. Sokirko, *Electrochim. Acta*, **39**, 597 (1994).
12. T. Ikeshoji and F. N. Nahui, *J. Electroanal. Chem.*, **305**, 147 (1991).
13. M. Ishizawa and T. Ogata, *Denki Kagaku*, **62**, 1054 (1994).

On the Origin of Electrochemical Oscillations at Silicon Electrodes

V. Lehmann*

Siemens AG, Department ZFE, 81730 Munich, Germany

ABSTRACT

Electrochemical oscillations at silicon electrodes anodized in hydrofluoric acid are a well known but poorly understood phenomena. It is less well known that potential oscillations are also observable during anodic oxidation in fluoride-free electrolytes. *In situ* measurements of stress, as well as x-ray reflectometry, atomic force microscopy, and ellipsometry were used to investigate the properties of the thin anodic oxide which covers the electrode surface during the oscillations. The results indicate a transition in the oxide morphology a thickness of about 10 nm. Based on this structural transition a model is developed which explains all observed features of the oscillation process in a consistent way.

Introduction

Since Faraday[1] proposed a thin oxide film to be responsible for the passivation of iron electrodes in sulfuric acid, many reactions at solid-state electrodes have been found to depend on the properties of anodic oxide films. Current oscillations at silicon electrodes under potentiostatic conditions in hydrofluoric acid (HF) were first reported by Turner in 1958.[2] In aqueous (HF) the electrochemical formation of an anodic oxide is accompanied by its chemical dissolution. This is different from the case of anodization in fluoride-free electrolytes where no dissolution occurs and the oxide thickness is monotonically increasing with anodization time. However, even in the second case oscillations of the potential were observed under galvanostatic conditions.[3,4] The origin of these electrochemical oscillations at silicon electrodes under anodic conditions is still unclear despite intensive research activities in this field.[5-13] It is the purpose of this work to give experimental evidence for an oscillation process which is based on a stress-induced transition of the anodic oxide morphology.

Experimental

Three different electrochemical setups were used in this work depending on the parameter under investigation. In order to record the current *vs.* voltage *i-V*, the voltage *vs.* time $V(t)$, or the current *vs.* time $i(t)$ characteristic a standard electrochemical cell with a Pt wire as a pseudoreference was used. The silicon samples were polished single crystalline <100> or <111> wafers. In order to avoid depletion of the electrode under anodic bias 1 to 10 Ω cm p-type or 3 mΩ cm n$^+$-type samples were used. All samples were

* Electrochemical Society Active Member.

HF dipped (hydrophobic) prior to anodization in order to remove the native oxide. The electrolyte for anodic oxidation was a 10 weight percent (w/o) aqueous solution of acetic acid. The dependence of the frequency of the oscillations on HF concentration was measured in aqueous HF. For oxide thickness measurements or stress measurements a 0.3 mol/kg ammonium fluoride was used. The pH of this solution was adjusted to 3.5 by adding H_2SO_4 in order to generate slow electrochemical oscillations of about 0.3 Hz.

The measurement of oxide thickness in acidic, fluoride containing electrolytes requires either *in situ* ellipsometry or a fast removal and rinsing of the samples for subsequent thickness measurements. The latter possibility was chosen and the cell design was optimized accordingly. A strip of silicon was mounted to a shaft as shown in Fig. 1. By rotation of the shaft the sample could be moved out of the electrolyte and rinsed with deionized water within about 0.1 s. For these experiments the active sample area was defined by a window (dotted area in Fig. 1) in a nitride layer of 100 nm thickness which covers the electrode.

In order to induce a measurable change of sample curvature by the growth of an anodic oxide layer of a few nanometers, very thin silicon samples are necessary. In addition, one side of the sample has to be protected against anodic oxidation. These requirements were fulfilled by using thin-stripe-shaped silicon samples with a nitride layer on the polished side as an anode. All thinning was done chemically by etching the samples in 50% KOH at 90°C to thicknesses below 30 μm. By using a beam splitter, two parallel laser beams (HeNe, 633 nm) are projected through the transparent Plexiglas (pmma) beaker onto the polished side of the sample (see Fig. 2). The distance of the reflected beams measured on a scale a few meters away, allows us to calculate the radius of curvature of the sample. For thin samples the sensivity of the setup is sufficient to monitor the change of curvature due to the growth of a few nanometers of anodic oxide.

Results

Electrochemical oscillations in fluoride-free as well as in fluoride containing electrolytes were investigated. Since anodic oxidation in fluoride-free electrolytes is not accompanied by chemical dissolution of the oxide, it is the simpler case and these results will be given first.

The voltage *vs.* time curve of a p-type <100> silicon sample anodized under a constant current density of 0.1 mA/cm^2 for $t > 0$ (sample was at OCP for $t < 0$) in 10% acetic acid is shown in Fig. 3. The periodic drop in the anodization potential which is reported by other authors[3,4] is clearly visible. A p-type sample of <111> crystal orientation which was anodized under the same conditions showed a voltage-time curve which was identical to the one of the <100> sample. In order to measure the thickness of the oxide, samples of <100> orientation were removed at

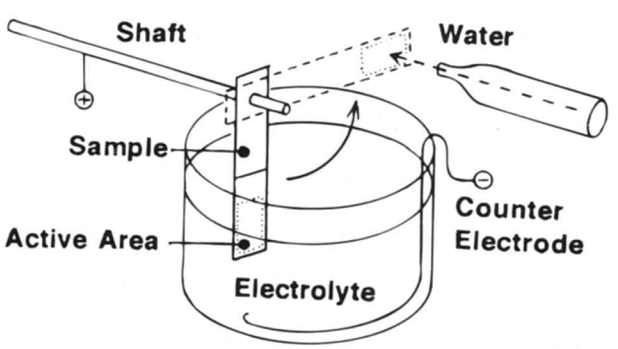

Fig. 1. This setup allows us to remove the anodized electrode from the electrolyte and rinse it with deionized water (broken arrow) within 0.1 s by fast rotation of the shaft (solid arrow). The active area of the electrode is defined by a window in a silicon nitride layer.

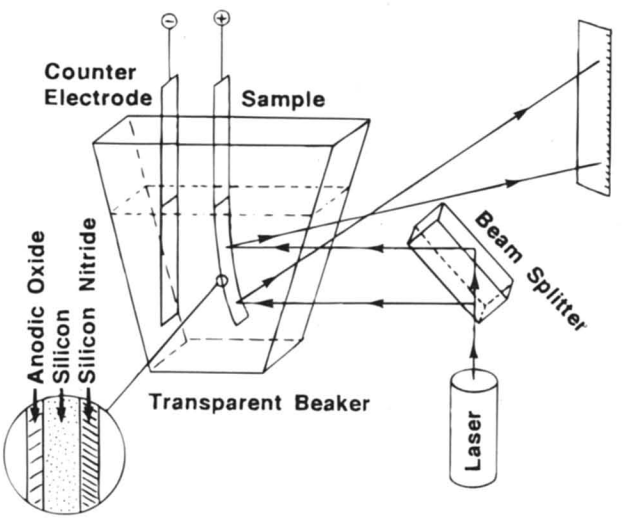

Fig. 2. The sketched setup is designed for *in situ* measurements of the stress, which is induced by the growth of an anodic oxide. The polished front side of the silicon electrode is protected against oxidation, while the back side is exposed to the electrolyte. From the deflection of two parallel laser beams the radius of curvature of the sample can be calculated.

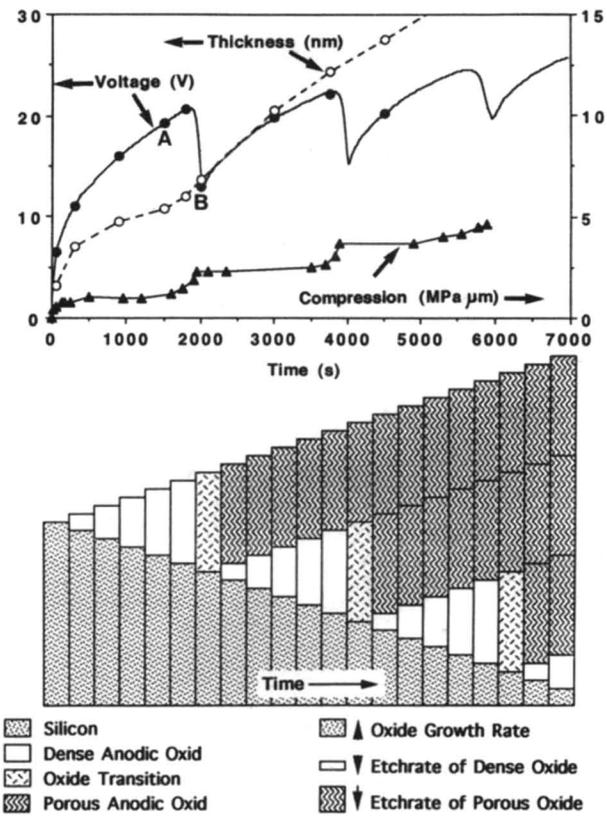

Fig. 3. Voltage *vs.* time curve for a p-type silicon electrode anodized with a constant current density of 0.1 mA/cm^2 in 10% acetic acid. Silicon electrodes were removed from the electrolyte after different times of anodization (solid circles) and the thickness of the anodic oxide was measured by ellipsometry (open circles, broken line fitted as a guide to the eye). Two of these samples, removed at points A and B, were investigated using x-ray reflectometry and AFM. The curvature of the sample was monitored during anodization and was used for the calculation of the compression (solid triangles). The bar graph sketch below the *V-t* curve visualizes the proposed formation mechanism.

certain points of the *V-t* curve (solid circles in Fig. 3) and measured by ellipsometry (open circles in Fig. 3). It is found, as expected, that the thickness of the oxide increases monotonically with time. However, the growth rate is not constant under galvanostatic conditions, indicating a contribution of other anodic reactions. The oxide growth efficiency is reported to be close to 100% during the first seconds of anodization, while it decreases below 20% for longer anodization times. This decrease is ascribed to the competing reaction of oxygen evolution.[14]

In order to get more information about the structure of the anodic oxide, two samples were removed before and after the first potential drop (point A and point B in Fig. 3) and analyzed using x-ray reflection. The results together with computer simulations are shown in Fig. 4. The angular reflectance of the oxide, which was removed before the potential drop, was best fitted by assuming a homogeneous oxide of 10.8 nm thickness and a density of 2.1 g/cm^3. The oxide removed after the drop was 13.1 nm thick and showed an angular reflectance which could be best fitted assuming a double-layer structure with a thin (2.9 nm), dense (2.1 g/cm^3) oxide at the silicon interface to the bulk silicon and a thick (10.2 nm), less dense (1.75 g/cm^3) oxide on top. Atomic force microscopy (AFM) of the surface of the oxidized samples, shown in Fig. 5, revealed a dramatic increase of the roughness (from sample A: 0.09 nm rms to sample B: 0.3 nm rms) during the potential drop. The topography of sample B shows a random ripple with a frequency of about 50 to 100 nm. Ellipsometry, as well as AFM measurements were performed at different spots of the same sample. No lateral variations of thickness or roughness were observed.

In order to measure the mechanical stress induced by the growing oxide, an *in situ* measurement of the bow of the sample was performed, using the setup shown in Fig. 2. The observed change of the radius of curvature R induced by the growth of an anodic oxide of the thickness d allows us to calculate the stress σ in the oxide film. Under the assumption that the strip is only deflected along one coordinate we obtain[15]

$$\sigma = -(E/(1 - \nu^2))\ (D^2/6Rd) \qquad [1]$$

where D is substrate thickness, ν the Poisson ratio (0.26), and E the Young's modulus (1.7×10^{12} dyn/cm^2) of the <100> oriented substrate.[16] The absolute value of the compressive stress in the 13.5 nm oxide after the first voltage minimum (Fig. 3, point B) calculated according to Eq. 1 was found to be about 175 MPa. A sample assumed to be deflected in two directions (circular plate) would increase the calculated stress values by 25% due to $(1 - \nu)$ being the denominator of the first factor in Eq. 1. A stress value of 175 MPa is comparable to values of intrinsic stress reported for low temperature (700°C) thermal oxides.[17,18] Since the thickness of the oxide could not be monitored during the *in situ* measurement of curvature, the stress-oxide thickness product (in MPa μm) is plotted in Fig. 3. This value will be designated compression and is proportional to $1/R$. The stress can be calculated by dividing the compression by the oxide thickness. Figure 3 shows that the compression increases very rapidly within the first 60 s of anodization. This time corresponds to an oxide thickness of 3.2 nm, as measured by ellipsometry or 4.4 nm, as calculated assuming an oxide density of 2.1 g/cm^3 and 100% growth efficiency. It is assumed that this rapid increase of compression within the first few seconds of anodization is due to the growth of the first monolayers of anodic oxide. However, a contribution in stress due to the change of the surface condition from hydrophobic to hydrophilic cannot be excluded. After this initial step, the compression remained constant within the measuring limits until the first potential maximum was reached. At the maximum and during the potential drop the next step-like change in compression was observed. This process continued periodically as shown in Fig. 3 (triangles). Thickness variations of the sample induced by inhomogeneous thinning in KOH will produce a certain error of the absolute values of stress, however, this is a systematic error. The relative error of the stress measurements is well below 10%.

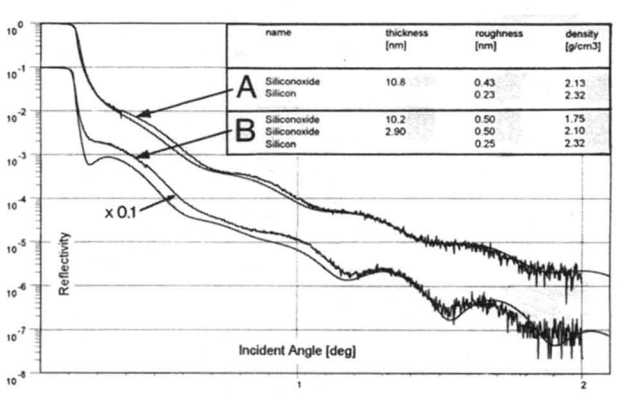

Fig. 4. X-ray reflectometry of anodic oxides grown according to Fig. 3, points A and B. The best agreement of the measured reflectivity (arrows) with the simulated reflectivity was obtained under the assumption of a single-layer structure for the anodic oxide on sample A and a bilayer structure for the oxide on sample B with values of thickness and density as shown in the legend of the figure.

Anodic oxide formation accompanied by its chemical dissolution is studied next. A chemical dissolution of the anodic silicon oxide requires an electrolyte which contains fluoride ions and has a low pH. The current voltage curve of a silicon electrode in a 0.3 mol/kg NH_4F solution of a pH of 3.5 (adjusted by adding H_2SO_4) is shown in Fig. 6. A variation of pH or concentration will change the absolute values of the current density minima and maxima, however the characteristic shape of the *i-V* curve does not change.[8] An anodic oxide layer is observed for current densities above J_{PS}. At different points of the curve (full circles in Fig. 6) silicon electrodes were quickly removed and rinsed in order to measure the oxide thickness by ellipsometry (open circles). At the second current density maximum (J_3) the oxide is about 3 nm thick. For more anodic bias the thickness increases rapidly to about 8 nm. Similar values of oxide thickness were found by charge measurements and capacitive methods.[6] Under potentiostatic conditions current oscillations are observed for potentials positive to the one corresponding to the second current minimum J_4 as shown in Fig. 6. Under galvanostatic conditions potential oscillations are observed for currents above J_3. Note that the thickness variation during the oscillation is minimal. This result is in accordance with *in situ* ellipsometry performed by other groups.[7,13]

It is reported that these current oscillations at silicon electrodes are damped and an exciting voltage or current step is required to generate them.[9] A change from damped to sustained potentiostatic oscillations is reported upon introduction of an uncompensated series resistance at the silicon electrode.[5] Sustained oscillations are observed in aqueous solutions of HF for concentrations above about 1.8% HF and below 5% HF. Below about 1.8% HF the oscillations are damped, while they become chaotic above 5% HF. No series resistance was added for these measurements, however, the contribution of the substrate (<0.1 Ω cm^{-2}) was not compensated. Figure 7 shows the dependence of the frequency of current oscillations on the average current density and the HF concentration of the electrolyte. The function is roughly linear corresponding to a constant value of charge of 13.3 mC/cm^2 exchanged per period. This charge corresponds to an anodic oxide thickness of 9.9 nm, assuming a density of 2.1 g/cm^3 and 100% growth efficiency. The exchanged charge is by orders of magnitude too large to be explained simply by charging effects. Even under the assumption of the maximum capacitance given by the Helmholtz layer (about 1 μF/cm^2) the stored charge would be much smaller.

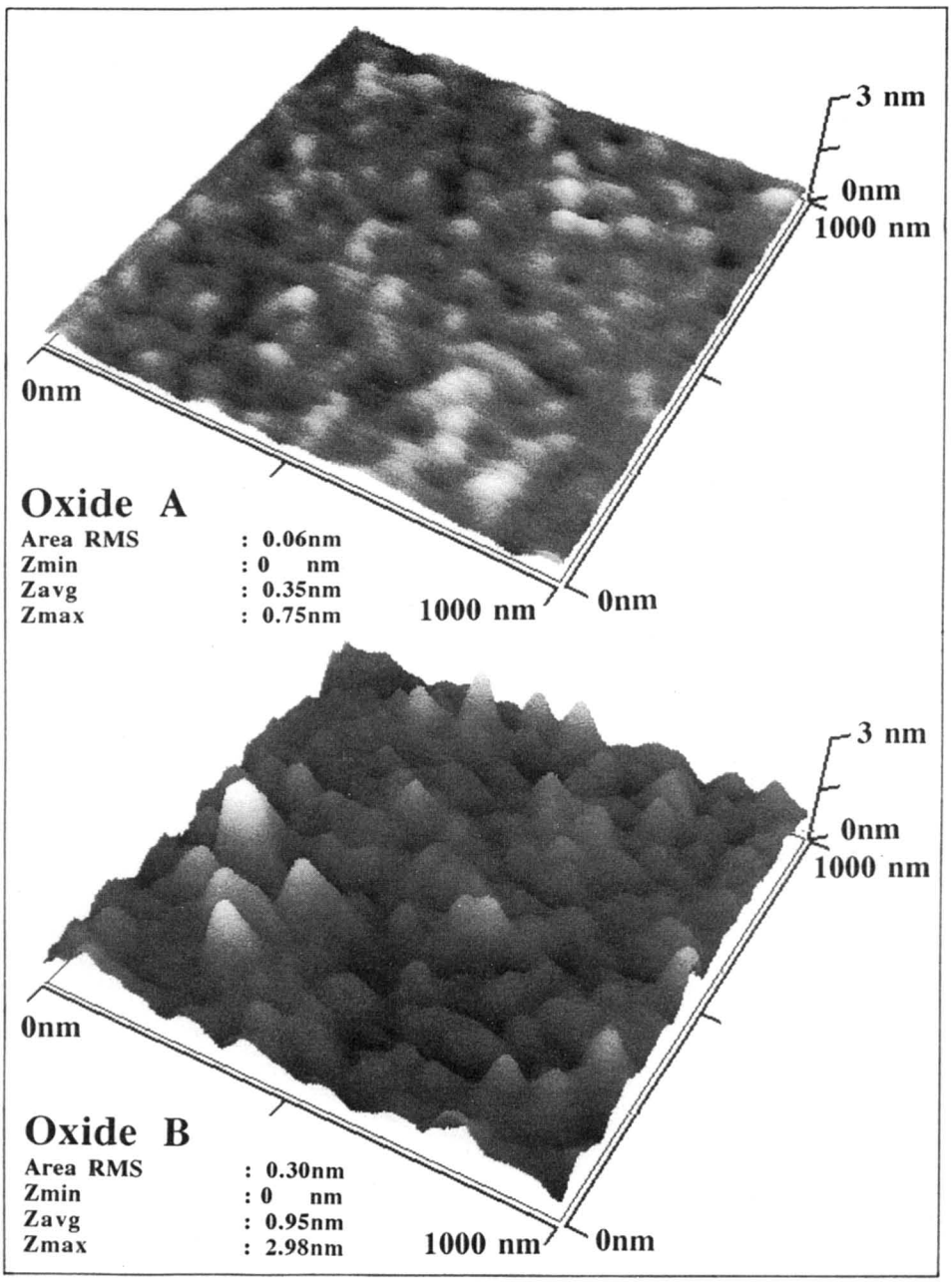

Fig. 5. Atomic force micrograph of the surface topograpy of anodic oxides before (A) and after (B) the potential drop shown in Fig. 3. The increase in surface roughness during the potential drop is clearly visible.

For the next experiment galvanostatic conditions were chosen because under constant current density the anodic oxide growth rate is constant. This can be concluded from the dissolution valence which is four in this regime,[19] indicating that the contribution of other anodic reactions like oxygen evolution is minimal. A potential *vs.* time curve for an n^+-type silicon electrode anodized with a constant current density of 6.25 mA/cm^2 for $t > 0$ (sample at OCP for $t < 0$) in 0.3 mol/kg NH_4F (pH 3.5) is shown in Fig. 8. The current density corresponds to a growth rate of 4.6 nm/s of oxide assuming a density of 2.1 g/cm^3. As shown in Fig. 8, the potential increases slowly until a charge value of about 55 mC/cm^2. Then a steep increase to about 8 V is observed. After the potential maximum the potential decreases in about 0.1 s to 1.5 V. The increase of potential to the next maximum occurs in about 4 s, which is the period for all following oscillations, corresponding to an exchanged charge of about 25 mC/cm^2 per period. At certain times (full circles in Fig. 8) samples were removed and rinsed using the setup shown in Fig. 1. The anodic oxide thickness of these samples as measured by ellipsometry is also shown in Fig. 8 (open circles, fitted by a broken line). It is found that the thickness variation under galvanostatic conditions during one period is below 2 nm. The curvature of the sample was monitored *in situ* using the setup shown in Fig. 2. As observed in the case of anodization in acetic acid a step-like increase of compression is observed in the first seconds of anodization. During the potential increase the compression was found to be constant. During the oscillations the change of curvature was surprisingly small, about 10% of the initial step which was close to the measuring limit. Therefore the exact compression-time-curve during the oscillations is not known. However, the maximum of compression was observed at the potential maximum.

In order to investigate if there is any influence of electric field on sample curvature, the current density was stepped to zero (open circuit potential, OCP) at certain points of the potential oscillation (arrows in Fig. 8). No change of compression was observed during this change of current density. After a delay of several seconds, however, the compression stepped down to the initial value. This was expected to occur because the anodic oxide is chemically etched in the electrolyte and after the removal of the last monolayer nothing is left to induce stress. The step-like manner in which stress relaxation occurs, makes it favorable for the determination of the oxide etch time as compared to other methods, as for example, the measure-

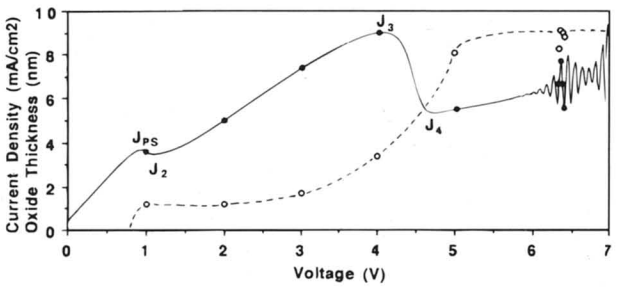

Fig. 6. The current density *vs.* voltage curve of a p-type Si electrode in NH_4F recorded with 50 mV/s. Current oscillations are observed in the potentiostatic regime for potentials positive of the one corresponding to the second current minimum (J_4). Under galvanostatic conditions the potential oscillates for current densities in excess of J_3. At the points indicated by full circles the electrode was quickly removed and the oxide thickness was measured by ellipsometry (open circles, broken line fitted as a guide to the eye).

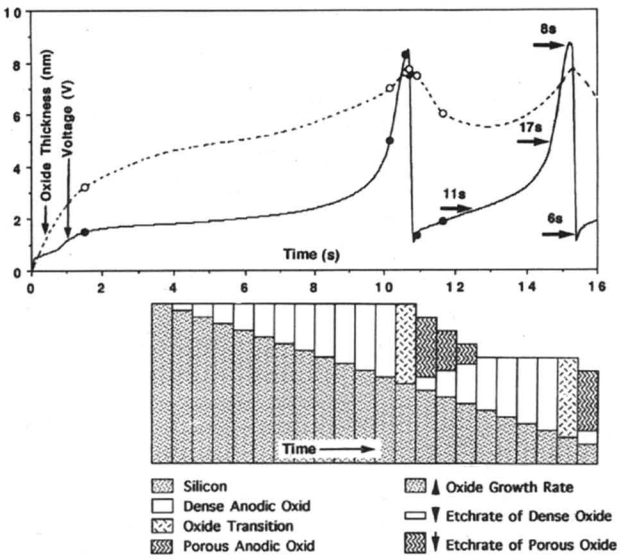

Fig. 8. Voltage *vs.* time curve (solid line) for an n^+-type silicon electrode anodized with a constant current density in NH_4F. The thickness of the anodic oxide was measured by ellipsometry (open circles, broken line fitted as a guide to the eye). The OCP dissolution time of the anodic oxide in the electrolyte was measured (values above arrows) at different points of the oscillation. The bar graph sketch below visualizes the proposed oscillation mechanism.

ment of the electron injection peak.[11] The delay times for complete etching of the anodic oxide (numbers at arrows in Fig. 8) were found to vary by a factor of three, while the oxide thickness variation is below 25%. The same results were obtained when the delay time between switching to OCP and the moment when the sample becomes hydrophobic was measured. The average etch rate of the anodic oxide, calculated from the delay times increases from about 0.4 to about 1.2 nm/s at the potential maximum. This average etch rate is still smaller than the growth rate of 4.6 nm/s which indicates that a very slow etching oxide phase of variable thickness is always present and dominates the etching time. This observation of a variation in oxide etch rate was a crucial point for the development of the oscillation model discussed below.

Discussion

The key to the understanding of the electrochemical oscillations at silicon electrodes is the thickness-dependent change in the morphology of the anodic oxide. For the discussion of the oscillation model it will only be assumed that during the morphological change from the flat, dense oxide to the rough, less-dense oxide the ionic permeability and the etch rate increase. The cause of the thickness-dependent change in the morphology is discussed after the presentation of the oscillation model.

The case of a silicon electrode which is anodized in a fluoride-free electrolyte is discussed first. The proposed oxide formation mechanism is visualized using a bar graph model as shown in the lower part of Fig. 3. The bars show the proposed oxide structure at the same time scale as the potential plotted above. The anodic growth of the dense oxide requires high electric field strengths up to values of about 17 MV/cm. If the potential across the oxide is constant over the whole sample area, which is fulfilled for a good conductivity of electrolyte and substrate, the oxide becomes very homogeneous in thickness. This is a self-adjusting process, because the electric field in a thin spot would be larger than the average value, generating a larger oxide growth rate until the average oxide thickness is reached at this spot. For a thick oxide spot the opposite is true. This effect synchronizes the oscillations. At about 11 nm the transition in the oxide morphology occurs (indicated by a change of the bar pattern in Fig. 3). After the transition the anodic oxide shows a high permeability and ions of the electrolyte penetrate the oxide. This leads to a sudden drop of the potential, if the electrolyte conductivity is large enough to "short-circuit" the electric field in the less dense oxide (bars with the wavy pattern in Fig. 3). If the electrolyte conductivity is too small, little or no oscillations will be observed.[3] During and after the potential drop the formation of a dense oxide continues at the interface next to the substrate which again leads to an increase of potential until this layer approaches a thickness of 11 nm and the next oxide transition occurs. Since the total thickness of the oxide increases monotonically, the oscillations are damped after a few periods.

In the case of an electrolyte which contains fluoride at low pH, the anodic oxide formation is accompanied by oxide dissolution. If the dissolution rate of the dense oxide is below its formation rate the thickness will increase, which leads to an increase of potential under galvanostatic conditions (as shown in Fig. 8). As in the case discussed above, the synchronization of the oscillations occurs during the potential increase because the potential does not vary spatially and consequently the oxide thickness becomes homogeneous across the sample surface. The transition of the dense oxide to the less dense modification enables ions to penetrate the oxide. This not only leads to the observed potential drop but also to enhanced etching of the oxide as shown in Fig. 8. Now the etch rate exceeds

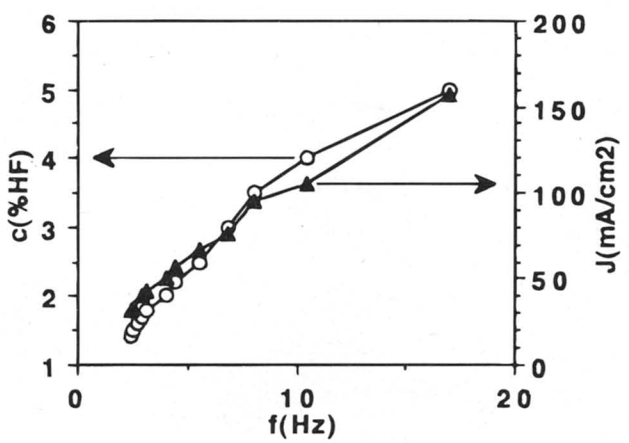

Fig. 7. The frequency *f* of potentiostatic electrochemical oscillations at a p-type silicon electrode in aqueous HF solutions shows a linear dependence on the concentration *c* (open circles) and the average current density *J* (solid triangles).

the growth rate and the total oxide thickness decreases until the less dense layer is etched away. The dense, slow etching oxide is exposed to the electrolyte again, and its thickness increases until the transition thickness is reached and so forth. This periodic process is shown in the bar graph sketch below the measured time *vs.* potential curve of Fig. 8. Note that the bar graph sketch of Fig. 8 was optimized to show oscillation periods according to the time scale of the observed potential oscillation above. Therefore the origin ($t = 0$) is not exactly modeled. The constant etch rate of the dense anodic oxide assumed in the model is also a simplification. As pointed out by Serre and co-workers[11] the etch rate of the very thin initial oxide, corresponding to J_3, is larger than the etch rate of the thicker oxide present at J_4. However, the quintessence of the presented model is not that the electrochemical reaction which forms the anodic oxide does oscillate, but that the oxide dissolution rate does, due to a change in oxide morphology.

This leads to the question of the microscopic nature of the change in the oxide morphology. The remarkable increase in surface roughness (Fig. 5) and the sudden increase in stress (Fig. 3) during the potential drop indicate an instability in oxide morphology rather than an electrochemical effect. Such a morphological instability was theoretically predicted for stressed solids[20] and recently observed for a thin SiGe-alloy which is under compression when deposited on a Si substrate.[21,22] A 10 nm thick, dislocation-free, nominally flat $Si_{0.5}Ge_{0.5}$ epi layer grown at 400°C was found to develop a random ripple pattern with a frequency of about 50 nm during a subsequent anneal at 560°C for 1 min. The authors argue that the coherent, highly compressed, initial layer is morphologically unstable and shows a transition to a dislocated, partially relaxed layer upon annealing.

For the observed transition in the anodic oxides a similar process is proposed: for oxide thicknesses in excess of 11 nm an inhomogenous distribution of the compressive stress becomes thermodynamically more favorable for the system than the homogeneous one. The observed rippled surface morphology (Fig. 4) is a consequence of the inhomogeneous distribution of stress, with areas of high stress and relaxed ones. From defect delineation in crystals it is known that etch rates are very sensitive to stress. Consequently the etch rate is assumed to be low for a homogenous distribution of compressive stress, while it becomes high after the transition to the rippled morphology.

Conclusions

The angular x-ray reflectivity and AFM measurements of anodic oxides grown on silicon electrodes shows a distinct transition from a dense, flat to a less dense, rippled modification at a certain thickness. Under galvanostatic conditions this transition is accompanied by a decrease of potential, an increase of stress, and an increase of etch rate. These observation give strong evidence that a stress dependent transition in oxide morphology occurs which is accompanied by a change in permeability for ions present in the electrolyte. The electrochemical oscillations observed in fluoride-free as well as fluoride containing electrolytes are a consequence of this transition in oxide morphology. Based on this transition a simple oscillation model for silicon electrodes is developed which may also shed some light on electrochemical oscillations observed at anodized electrodes of other materials.

Acknowledgments

Stimulating discussions with U. Grüning, B. Jobst, W. Hösler, and U. Gösele are gratefully acknowledged.

Manuscript submitted April 10, 1995; revised manuscript received Sept. 1, 1995.

Siemens AG assisted in meeting the publication costs of this article.

REFERENCES

1. M. Faraday, *Philos. Trans. R. Soc., Ser. A*, **124,** 77 (1834).
2. D. R. Turner, *This Journal,* **105,** 402, (1958).
3. V. P. Parkhutik, *Electrochim. Acta*, **36,** 1611, (1991).
4. M. J. Madou, W. P. Gomes, F. Fransen, and F. Cardon, *This Journal,* **129,** 2749 (1982).
5. J.-N. Chazalviel, F. Ozanam, M. Etman, F. Paolucci, L. M. Peter, and J. Stumper, *J. Electroanal. Chem.*, **327,** 343 (1992).
6. J.-N. Chazalviel, *Electrochim. Acta*, **37**, 865 (1992).
7. J. Stumper, R. Greef, and L. M. Peter, *J. Electroanal. Chem.*, **310,** 445 (1991).
8. J.-N. Chazalviel, M. Etman, and F. Ozanam, *ibid.*, **297,** 533 (1991).
9. F. Ozanam, J.-N. Chazalviel, A. Radi, and M. Etman, *Ber. Bunsenges. Phys. Chem.*, **95,** 98 (1991).
10. J.-N. Chazalviel and F. Ozanam, *This Journal,* **139,** 2501 (1992).
11. C. Serre, S. Barret, and R. Herino, *ibid.*, **141,** 2049 (1994).
12. H. Gerischer and M. Lübke, *Ber. Bunsenges. Phys. Chem.*, **92,** 573 (1988).
13. M. Aggour, M. Giersig, and H. J. Lewerenz, *J. Electroanal. Chem.*, **283,** 67 (1995).
14. J. A. Bardwell, K. B. Clark, D. F. Mitchell, D. A. Bisaillion, I. G. Sproule, B. MacDougall, and M. J. Graham, *ibid.*, **140,** 2135 (1993).
15. A. C. Ugural, *Stresses in Plates and Shells,* McGraw-Hill, New York (1981).
16. K. Barla, R. Herino, G. Bomchil, J. C. Pfister, and A. Freund, *J. Cryst. Growth*, **68,** 727 (1984).
17. E. Kobeda and E. A. Irene, *J. Vac. Sci. Technol.*, **B4,** 720 (1986).
18. E. Kobeda and E. A. Irene, *ibid.*, **B5,** 15 (1987).
19. V. Lehmann, *This Journal,* **140,** 2836 (1993).
20. W. H. Yang and D. J. Srolovitz, *Phys. Rev. Lett.*, **71,** 1593 (1993).
21. D. E. Jesson, S. J. Pennycook, J.-M. Baribeau, and D. C. Houghton, *ibid.*, **71,** 1744 (1993).
22. D. E. Jesson, K. M. Chen, S. J. Pennycook, T. Thundat, and R. J. Warmack, *Science,* **268,** 1161 (1995).